Materials Research. 2021; 24(6): e20210086
DOI: https://doi.org/10.1590/1980-5373-MR-2021-0086

Investigation of Structural, Electronic and Optical Properties of $Na_2InAgCl_6$, $K_2InAgCl_6$, and $Rb_2InAgCl_6$ Lead-Free Halide Double Perovskites Regarding with $Cs_2InAgCl_6$ Perovskites Cell and a Comparative Study by DFT Functionals

***Md. Hazrat Ali*[a], *Mohammad Jahidul Islam*[b], *Ajoy Kumer*[c,d]*, *Md. Sayed Hossain*[e], *Unesco Chakma*[a], *Debashis Howlader*[a], *Md. Tawhidul Islam*[a], *Tomal Hossain*[a]**

[a]*European University of Bangladesh, Department of Electrical and Electronics Engineering, Gabtoli, Dhaka-1216, Bangladesh.*
[b]*European University of Bangladesh, Department of Physics, Gabtoli, Dhaka-1216, Bangladesh.*
[c]*European University of Bangladesh, Department of Chemistry, Gabtoli, Dhaka-1216, Bangladesh.*
[d]*Bangladesh University of Engineering and Technology, Department of Chemistry, Dhaka-1000, Bangladesh.*
[e]*Bangladesh Atomic Energy Commission, Center for Research Reactor, Dhaka, Bangladesh.*

Received: February 13, 2021; Revised: July 06, 2021; Accepted: September 18, 2021

Electronics band structures, the total density of state, the partial density of state and optical properties were investigated by DFT method for $A_2InAgCl_6$ (A= Cs, Na, K, and Rb). Moreover, the band gap of $Na_2InAgCl_6$, $K_2InAgCl_6$, $Rb_2InAgCl_6$ and $Cs_2InAgCl_6$ were calculated at 1.039 eV, 1.041 eV, 1.039 eV and 1.089 eV by GGA with PBE, 0.784 eV, 0.769 eV, 0.775 eV and 0.770 eV by LDA with CA-PZ and 1.310 eV, 1.152 eV, 1.180 eV and 1.169 eV by GGA with RPBE functionals. The density of states (DOS) and partial density of states (PDOS) were evaluated. Among of used functionals, GGA with RPBE functional has considered the appropriate and acceptable method for calculation of band gap where the 1.310 eV of band gap was reported for $Cs_2InAgCl_6$, which is close to experimental value at 1.370 eV. The crystal, $Na_2InAgCl_6$, has considered as the best perovskites cell among other four due to low band gap, and the main cause is revealed that it has attached the lightest Na atom to convey the low band gap as lower surface or atomic size atom.

Keywords: *Band structure, density of states, optical properties and DFT method.*

1. Introduction

Photovoltaic application owing to their excellent structural stability and tunable band gap in the visible range for lead-free halides has a great potential value to researcher as well as industries. Organic–inorganic hybrid perovskites of lead-halide have prospered as one family of the most expectant optoelectronic materials[1,2] where organic ligand methylamine was used as unique organic high end[3], on account of their unique features for high absorption coefficients, diffusion lengths of long carrier and low processing cost[4,5], and it might be introduced as low-priced device for future prospective and simple preparation ways[6,7]. Optoelectronic devices have been successfully achieved by various lead halides perovskites based, including solar cells[8], light emitting diodes[9], lasers[10], as well as photo detectors for near infrared, ultraviolet, and visible light detections[11,12]. The efficiency of these perovskite cell materials grow steadily while there are two residual challenges that need to be addressed in order to use perovskites solar cells for electricity production in presence of toxic lead and its stability[13-15]. On the front of lead metal replacement, several lead-free perovskites solar cells of methyl ammonium based on lead-iodide and related materials showed an unparalleled growth in power conversion efficiency, up to a carried record exceeding 22%[14,16,17]. However, despite this astonishing success, solar cells of perovskites are also facing significant challenges, due to the lack of stability upon prolonged exposure to light, humidity, and increased temperatures.

Recently, $Cs_2BiAgBr_6$ is static up to 703K without any phase transition. However, lead-free halides $Cs_2BiAgBr_6$ and $Cs_2BiAgCl_6$ are still unsuitable for photovoltaic applications because of their indirect band gap[18,19]. Due to indirect band gap, the transferring the energy from valance band to conduction band is not so easy, and there is created a barrier force which leads the own electric conductivity, resistance and magnetic field, as a result it loses it's excellency in the uses of lasers, optoelectronics, perovskites solar cells[20]. Solving these problems by a band structure engineering concept, this brings indirect band gap to the transition of the direct band gap. Lately, G. Volonakis et al.[21], have narrated another lead-free double halide perovskites $Cs_2InAgCl_6$. The new Indium (In) based double perovskites has a greatly tunable direct band gap for visible range. The synthesized powders of $Cs_2InAgCl_6$ were pointed out white coloration, and its optical band gap was 3.3 eV. Regarding the photo-luminescence emission energy, it

*e-mail: kumarajoy.cu@gmail.com

is essential staying the band gap about 2.0 eV[22,23]. Moreover, numerous experimental and computational studies on the optoelectronics properties of $Cs_2InAgCl_6$ have been studied to disclose the correctness of its photovoltaic applications[21,24]. However, optical properties of $A_2InAgCl_6$ (A= Cs, Na, K, and Rb) have still remained unexplored. The double metal halide perovskites (MHPv) $A_2InAgCl_6$ (A= Cs, Na, K, and Rb) are direct band gap semiconductor and proclaim good optical properties. Consequently, it is fascinating to studies of a first principle approach of $A_2InAgCl_6$[21,24].

This paper describes the first-principles calculations to identify double metal halides perovskites (MHPv) with direct band gaps. In reference of $Cs_2InAgCl_6$, it has changed the Cs metals by Na, K and Rb to make a comparative study through Group I alkali metals by DFT method. It is well known problem for GGA with PBE and LDA with (CA-PZ) that it introduces a deviation of their electronic structure calculation due to producing the magnetic field in optimization[25,26]. Regarding this problem, the GGA with RPBE method has executed in this study and compared with its experimental value for getting its accuracy and validation[27,28]. As a result, GGA with RPBE has been used for calculating the optical properties with same setting option for $Cs_2InAgCl_6$, $Na_2InAgCl_6$, $K_2InAgCl_6$, and $Rb_2InAgCl_6$ crystals.

2. Computational Methods

The method of GGA with PBE was optimized from CASTEP code of the material studio version 8.0[29], and it was used to compute the band structure, total density of state (TDOS) and partial density of state (PDOS), because it has been considered the most feasible method for calculating the electronic and structural properties[27]. In this condition, the band structure and density of state were enumerated using the cut off at 490 eV, and k point at 2×2×2 with nom-conserving pseudopotentials. Then the optical features were similar way simulated for calculation of the refractive index, reflectivity, absorption, conductivity and loss function. Moreover, the geometric optimization was achieved before energy calculation, and the convergence criterion for the force between atoms was 3×10^{-6} eV/A˚. The maximum displacement was 1×10^{-3}A˚, and the total energy and the maximal stress were 1×10^{-5} eV/atom and 5×10^{-2} GPa, respectively. In addition, for the comparative study of band gaps for $Cs_2InAgCl_6$, $Na_2InAgCl_6$, $K_2InAgCl_6$ and $Rb_2InAgCl_6$, the other two common methods, such as Local Density Approximation (LDA) with Ceperley and Alder and Perdew and Zunger (CA-PZ)[25] and Generalized Gradient Approximation (GGA) with Revised Perdew-Burke-Ernzerhof (RPBE)[28] functionals had investigated using required cut off energy at 490 eV, and k point at 2×2×2 with nom-conserving pseudopotentials of required structures.

3. Results and Discussion

3.1. Geometry of optimized structure

The lattice parameter values for $Cs_2InAgCl_6$ are calculated from the materials studio after optimizing their crystal structure which are listed in the Table 1 as the basic structural units through the three methods, and try to keep its similar parameters getting a comparative study at a point. Withal, it must be noted for optimization structure showing in Figures 1a to 1d which were taken after simulation GGA with RPBE which has been considered as the standard functional of DFT having heavy metal atoms in crystal. But the GGA with PBE, which has estimated the most accurate and acceptable DFT functional for calculating the electronic structure of heavy metals containing crystals[30-34] shows very close magnitude of band gap.

3.2. Electronic structure

To ascertain the electronic band structure of the $Cs_2InAgCl_6$, $Na_2InAgCl_6$, $K_2InAgCl_6$, and $Rb_2InAgCl_6$, the Fermi energy level was set as zero. From the Figures 2a to 2l, it was discovered that the minimum of conduction bands (MCB) were obtained in the G symmetry point whereas the maximum of valance bands (MVB) were linked also in G symmetry points. It was observed the direct band gap as the both of MCB and MVB are at point G symmetry and evaluated by 1.089 eV, 1.038 eV, 1.041 eV and 1.039 eV respectively using GGA with PBE for $Cs_2InAgCl_6$, $Na_2InAgCl_6$, $K_2InAgCl_6$, and $Rb_2InAgCl_6$ shown in Figures 2a to 2d. It can be seen that both upper and lower parts of the conduction band are well dispersive in the near W, L, and X symmetry points than T and K symmetry point. Contrariwise, the upper level of the valance band is highly dispersive for $Na_2InAgCl_6$. Also, both of the upper and lower segments of the conduction band are well divergent in the near W, L, G, and X symmetry points than T and K symmetry point. On the other side, the upper segment of the valance band near the G symmetry point is equally dispersive; however, the lower part is not divergent. At every turn, the effective mass of the lower carrier corresponds to higher carrier mobility.

Besides, LDA with CA-PZ was applied for investigation of the band gap of $Cs_2InAgCl_6$, $Na_2InAgCl_6$, $K_2InAgCl_6$ and $Rb_2InAgCl_6$ from Figures 2e, 2f, 2g, and 2h. It can be seen that all band gap are direct band gap which shows a large similarity to the enumerated method GGA with PBE. The band gaps of metal halide perovskites are 0.784, 0.769, 0.775, and 0.770 eV for $Cs_2InAgCl_6$, $Na_2InAgCl_6$, $K_2InAgCl_6$ and $Rb_2InAgCl_6$, respectively.

Ultimately, GGA with RPBE was demonstrated for calculated the band gap with the same required condition and listed in Figures 2i, 2j, 2k, and 2l. It has illustrated that all metals halide perovskites (MHPv) shows the direct

Table 1. Structural calculation by three methods of $Cs_2InAgCl_6$.

Methods	a	b	c	α	β	γ	Crystal type	Space group	Density
GGA, PBE	7.538Å	7.538Å	7.538Å	60.0°	60.0°	60.0°	cubic	Fm $\overline{3}$ m [225]	3.84 g/cm^3
LDA, CA-PZ	7.538Å	7.538Å	7.538Å	60.0°	60.0°	60.0°	cubic	Fm $\overline{3}$ m [225]	3.84 g/cm^3
GGA, RPBE	7.538Å	7.538Å	7.538Å	60.0°	60.0°	60.0°	cubic	Fm $\overline{3}$ m [225]	3.84 g/cm^3

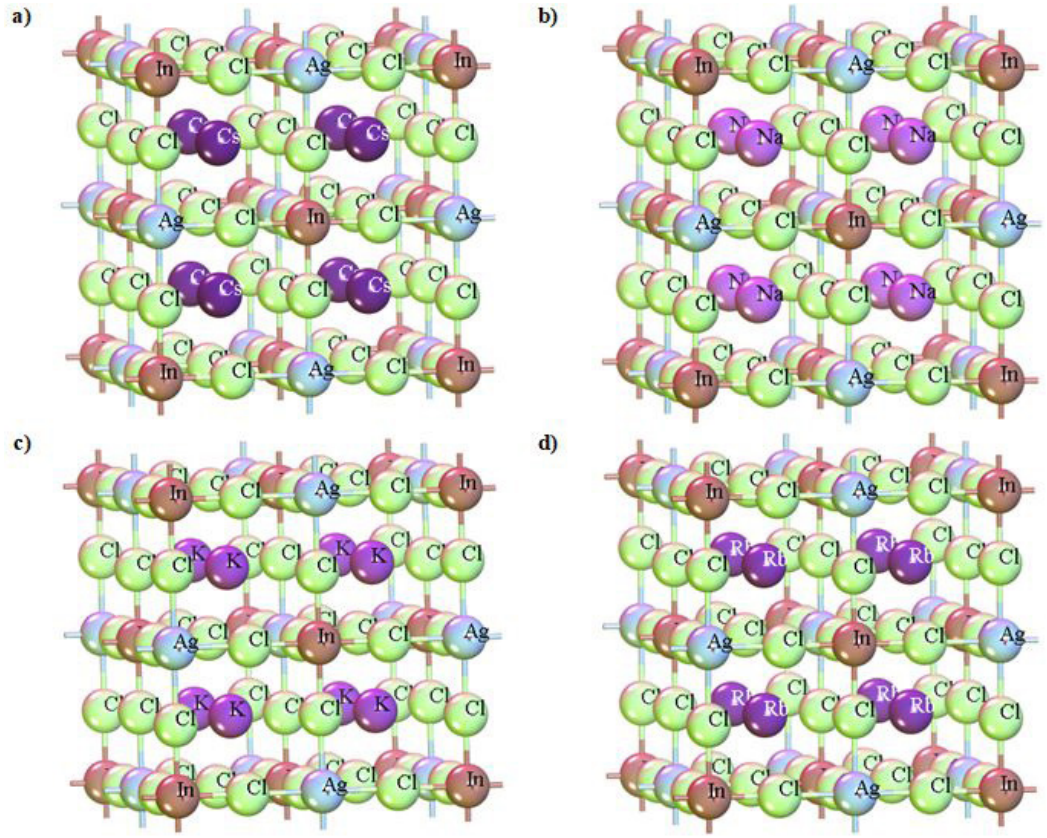

Figure 1. a) Optimized structure of $Cs_2InAgCl_6$, b) Optimized structure of $Na_2InAgCl_6$, c) Optimized structure of $K_2InAgCl_6$, and d) Optimized structure of $Rb_2InAgCl_6$.

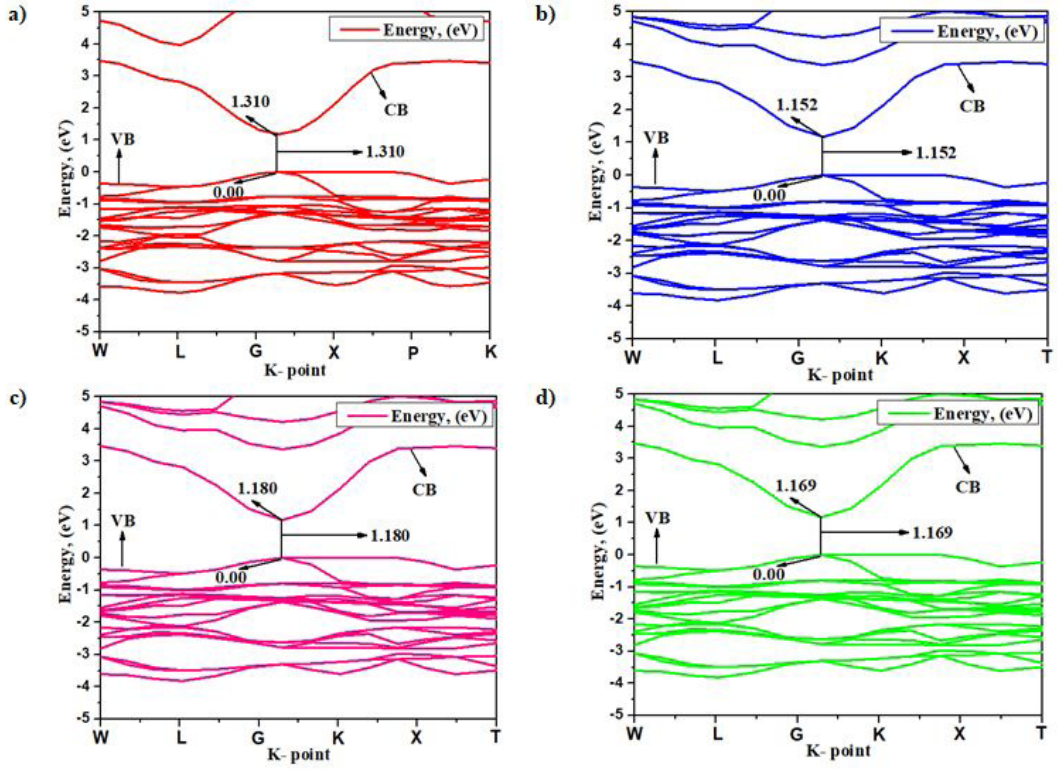

Figure 2. a) Band structure for $Cs_2InAgCl_6$, b) Band structure for $Na_2InAgCl_6$, c) Band structure for $K_2InAgCl_6$, and d) Band structure for $Rb_2InAgCl_6$.

band gap and the magnitude are 1.310, 1.152, 1.180, and 1.169 in eV for $Cs_2InAgCl_6$, $Na_2InAgCl_6$, $K_2InAgCl_6$ and $Rb_2InAgCl_6$, respectively. The comparative values of optimized conditions are listed in Table 2. In the view of GGA with RPBE give almost similar value of experimental value for reference crystal, $Cs_2InAgCl_6$, in matarialsproject.org linked to https://materialsproject.org/materials/mp-1096926/#snl, and ID is mp-1096926[35]. As a result, GGA with RPBE has the standard method in this study for further investigation.

3.3. Density of states and Partial density of state

The density of state and partial density of state were simulated for evaluating the nature of $5s^2$, $5p^6$ and $6s^1$ for Cs, $2s^2$, $2p^6$ and $3s^1$ for Na, $3s^2$, $3p^6$ and 4s1 for K, $4s^2$, $4p^6$ and $5s^1$ for Rb, $4d^{10}$, $5s^2$ and $5p^1$ for In, $4s^2$, $4p^6$ and $4d^{10}$ for Ag, $3s^2$ and $3p^5$ for Cl atom of $A_2InAgCl_6$ orbitals which can be travelled from maximum valance band (MVB) to the minimum conduction band (MCB) due to hybridization. The density of state indicates the nature of electronic band structures and scattering of the orbital. The total density of states (DOS) of A (Cs, Na, K, Rb), In, Ag, and Cl elements for $A_2InAgCl_6$, crystals have been calculated by GGA with PBE. From Figures 3a to 3p depicted the DOS and PDOS are directly involved with the chemical reactivity descriptors, such as Highest Occupied Molecular Orbital (HOMO), Lowest Unoccupied Molecular Orbital (LUMO), HOMO-LUMO gap those three indicators are used to calculated ionization potential, electronegativity, hardness, softness and electron affinity of any crystals[36,37]. Positive part of energy for density of states indicates the LUMO and negative segment of energy mentions the HOMO. HOMO trends to attract the nucleophilic and LUMO trends to attract the electrophilic.

According to quantum mechanics, the terms HOMO and LUMO are utilized to framework with quantum physics while the terms conduction band and valance band are exploited on behalf of classical physics. In addition, HOMO is equivalent for valance band while LUMO is correspondent to the conduction band. The difference of the CB-VB is band gap and on similar terms, LUMO-HOMO is the band gap, and is energy levels required for the conduction to take place[38-42]. As a result, DOS and PDOS employ the calculation of HOMO, LUMO for all containing orbitals for $Cs_2InAgCl_6$, $Na_2InAgCl_6$, $K_2InAgCl_6$ and $Rb_2InAgCl_6$, respectively.

In addition, the comparative study of DOS for $Cs_2InAgCl_6$, $Na_2InAgCl_6$, $K_2InAgCl_6$, and $Rb_2InAgCl_6$ metal halide perovskites (MHPv) crystals and interprets that $Na_2InAgCl_6$, $K_2InAgCl_6$, and $Rb_2InAgCl_6$ showing the highest density of electron in valance band than $Cs_2InAgCl_6$ depicted in Figure 3a.

Form the Figures 3b to 3m illustrates the PDOS for $Cs_2InAgCl_6$, $Na_2InAgCl_6$, $K_2InAgCl_6$ and $Rb_2InAgCl_6$,

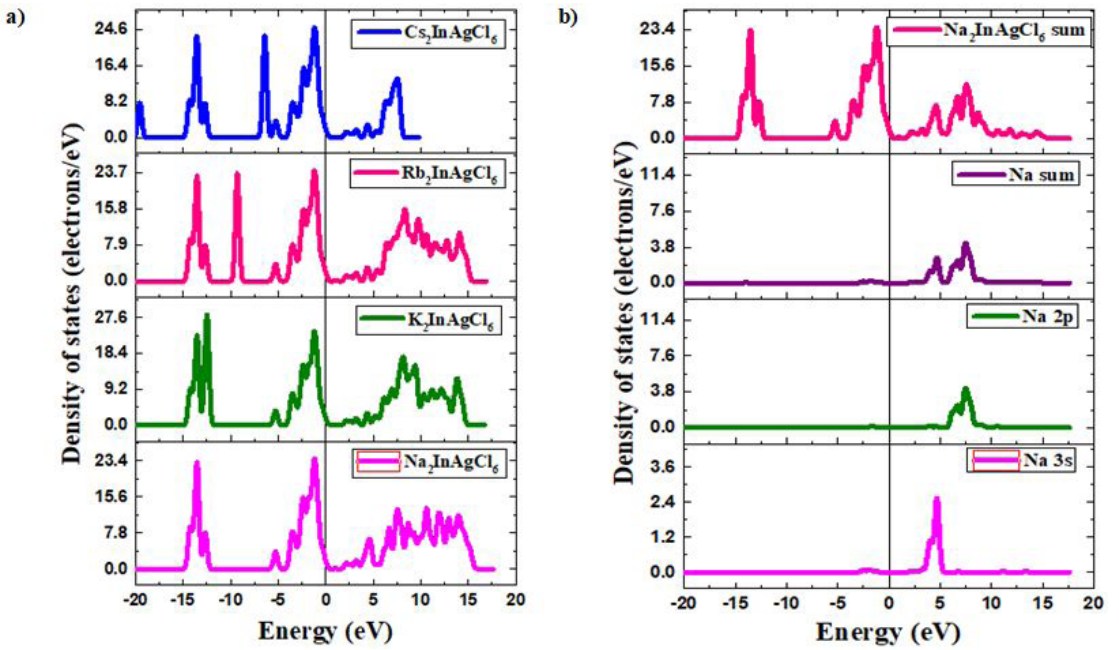

Figure 3. a) Comparison of total DOS for $A_2InAgCl_6$ (A=Cs, Na, K, Rb), and b) PDOS $Na_2InAgCl_6$ for Na atom.

Table 2. Band gap in eV for $Cs_2InAgCl_6$, $Na_2InAgCl_6$, $K_2InAgCl_6$ and $Rb_2InAgCl_6$.

Crystal	GGA, PBE	LDA, CA-PZ	GGA, RPBE	Experimental value
$Cs_2InAgCl_6$	**1.089**	**0.784**	**1.310**	**1.370** as direct band gap[21]
$Na_2InAgCl_6$	1.038	0.769	1.152	Newly predicted
$K_2InAgCl_6$	1.041	0.775	1.180	Newly predicted
$Rb_2InAgCl_6$	1.039	0.770	1.169	Newly predicted

respectively. We found that the density of state were simulated for evaluating the nature of $5s^2\ 5p^6\ 6s^1$ for Cs, $2s^2\ 2p^6\ 3s^1$ for Na, $3s^2\ 3p^6\ 4s^1$ for K, $4s^2\ 4p^6\ 5s^1$ for Rb, $4d^{10}\ 5s^2\ 5p^1$ for in, $4s^2$, $4p^6$, $4d^{10}$ for Ag, $3s^2\ 3p^5$ for Cl atom for $A_2InAgCl_6$. As orbital's traveling with the maximum valance band (MVB) to the minimum conduction band (MCB) to explain the transition of electrons owing to hybridization. The p orbital has the higher portion among others in both of valance band and conduction band. The $5p^6$ orbital are totally vacant so that it trends to conduction band while P atom has partial fill up the $2p^6$ orbital as a result the highest peak for PDOS of conduction band is obtained for p orbital. Moreover, the PDOS of p orbital in the conduction band almost equal to DOS. So it can be said that the conduction band consists of $5p^6$ of Cs, $2p^6$ of Na, $3p^6$ of K, $5p^1$ of Rb, $4p^6$ of Ag, and $3p^5$ of Cl atom even the valance band contains mixing of p, s and d orbital's. The density of electron in valance band exhibits higher for p orbital than d orbital. On the other side, the electrons density of the conduction band is around 25 electrons/ eV while p orbital is the response for about 20 electrons/ eV.

Furthermore, the comparative study of s, p, and d orbital for $Cs_2InAgCl_6$, $Na_2InAgCl_6$, $K_2InAgCl_6$ and $Rb_2InAgCl_6$, displayed in Figures 3n, 3o, and 3p respectively. The Figure 3n interprets s orbital's are almost same for $Cs_2InAgCl_6$, $Na_2InAgCl_6$, and $K_2InAgCl_6$, but $Rb_2InAgCl_6$ is solidly high. The contribution of s and p orbitals in $Cs_2InAgCl_6$, $Na_2InAgCl_6$, $K_2InAgCl_6$, and $Rb_2InAgCl_6$ is approximately equal but it is different for the d orbital. The s and p orbital is the higher contributor for the conduction band of $A_2InAgCl_6$ and those are the key cause for decreasing the band gap and promoting good perovskites activity.

3.4. Optical properties

3.4.1. Optical reflectivity

As a segment of several consecutive theoretical investigations of optical phenomenon, firstly, for analysis of the quantification of optical reflectivity for crystalline material, it has played a vital role in the electronic shifting from valance band to the conduction band. The amount of light if falling as incident ray on the surface of the semiconductor materials can be estimated from the reflectivity data which is recounted to the absorbance of that material. It has reported in a some of previous investigations in our research that the lower reflectivity indicates the higher UV or visible light absorption. In our research, the reflectivity of $Cs_2InAgCl_6$, $Na_2InAgCl_6$, $K_2InAgCl_6$ and $Rb_2InAgCl_6$ was initiated from around 0.40, 0.41 and 7 eV, 17 eV, respectively at inaugural reflectivity and frequency for $Cs_2InAgCl_6$ and $Na_2InAgCl_6$, after a successive aggrandizement it reached a falling down of 0.02 and 0.03 at 12 eV and 15eV and gradually falling in about 0.02 corresponding frequency at 15 eV as depicted in Figure 4. There was changing at different point of $Cs_2InAgCl_6$, $Na_2InAgCl_6$, $K_2InAgCl_6$, and $Rb_2InAgCl_6$, but $Cs_2InAgCl_6$ and $Na_2InAgCl_6$ shows larger reflectivity than $K_2InAgCl_6$ and $Rb_2InAgCl_6$. It is worth mentioning that, the value of reflectivity saw a dramatic zigzag between 0 to 12 eV, after that all MHPv experienced a linear constant fashion except for $K_2InAgCl_6$.

3.4.2. Absorption

The method of polarization for polycrystalline is utilized to evaluate the optical absorbance of the $Cs_2InAgCl_6$, $Na_2InAgCl_6$, $K_2InAgCl_6$, and $Rb_2InAgCl_6$ material. During the simulation, a small smearing value of 0.1 was applied to attain more distinguishable absorbance peaks. The discovered absorbance peaks as depicted in Figure 5 are attributed to the photo transition energies from the maximum valance band (MVB) to the minimum conduction band (MCB) under visible light irradiation which suggests that this material can absorb photons of visible range. It was discovered that the absorption rate for $Na_2InAgCl_6$, $K_2InAgCl_6$, and $Rb_2InAgCl_6$ exhibits greater than $Cs_2InAgCl_6$ after photon energy 10 eV. Since, we substituted Cs with Na, K, and Rb and observed that the size of the atom plays a significant role in larger absorbance. Consequently, the predicted MHPv shows remarkable photocatalytic activity due to its vast absorption obtained Figure 5 although it might be good UV light absorbance.

3.4.3. Reflective index

The refractive index of a material is an impactful parameter for measuring the photon absorption throughout the process of chemicals degradation from the solutions. A large value

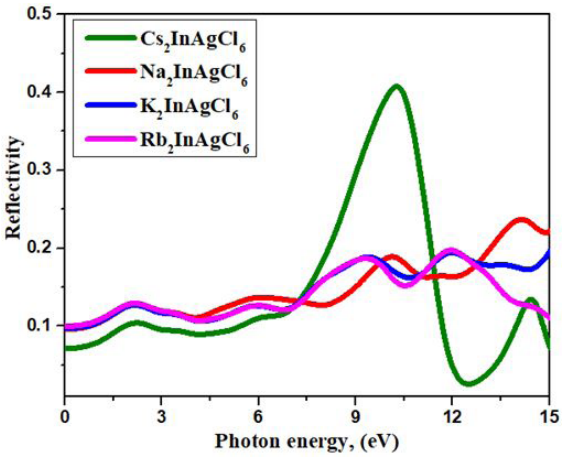

Figure 4. Reflectivity.

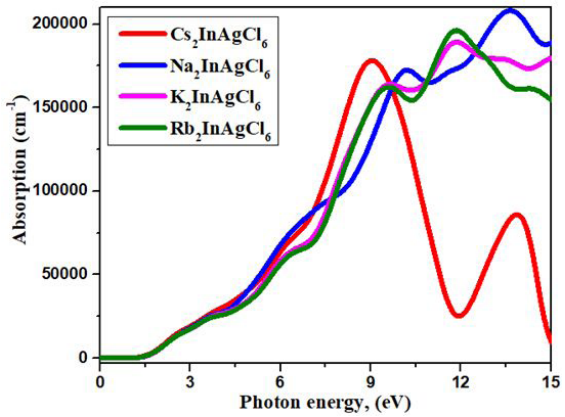

Figure 5. Absorption.

of the refractive index is associated with the greater denser medium which is reported in a previous investigation[43-48]. The real part and the imaginary part for both of the $Cs_2InAgCl_6$, $Na_2InAgCl_6$, $K_2InAgCl_6$ and $Rb_2InAgCl_6$ of refractive index are mentioned in Figures 6a and 6b as a function of photon energy. In view of a diagram showing an inverse pattern at an initial point of photon energy, as well as the refractive index is higher for the real part while the imaginary part is almost closed to zero. Finally, the decrease of both parts encounters them to each other up to 7 eV photon energy with a value of the refractive index is 1.2 and afterward, they follow a constant pattern with slightly different values of refractive index.

3.4.4. Dielectric function

The dielectric function is an fundamental contrivance to inspect their optical properties which are relayed to adsorption properties as the subsequent equation for materials[49].

$$\varepsilon = \varepsilon_1(\omega) + i\varepsilon_2(\omega)$$

Where, ε_1 (ω) and ε_2 (ω) are denoted the dielectric constant (real part) and the dielectric loss factor (imaginary part), respectively. The relationship with space of materials is related to the dielectric function that is physically equivalent to the permittivity or absolute permittivity. The real part of dielectric function illustrates the energy storage potential in the electric field and the imaginary part signifies the energy dissipation aptitude of the dielectric materials. In Figures 7a and 7b, the imaginary part is less than the real part form 0 eV to 5 eV frequencies; however, from 6 eV to 15 eV the imaginary part is larger than the real part, showing same the real and imaginary part for $Cs_2InAgCl_6$, $Na_2InAgCl_6$, $K_2InAgCl_6$, and $Rb_2InAgCl_6$.

3.4.5. Conductivity

The energy gap between the valence band and conduction band for semiconductors is poorer than insulators so that, semiconductors are likely to a semi-good electrical conductor whereas their valence band is entirely empty. The conductivity of materials is on the inevitable part of the energy band and orbital's electrons are associated with the discrete space of electrons in orbit. In the crystal molecules, it is also produced by the presence of holes and free electrons. The conductivity of $Na_2InAgCl_6$, $K_2InAgCl_6$ and $Rb_2InAgCl_6$ is slightly higher than $Cs_2InAgCl_6$ as shown in Figures 8a and 8b. So, the real part shows that the highest conductivity peak reached at 3.5 by 10 eV and for imaginary part 2.5 by 15 eV for $Na_2InAgCl_6$. The conductivity has recorded as increased for substituting Cs by Na, K, and Rb for both real and imaginary parts so that it is the significant turning point of this research.

3.4.6. Loss function

The electronic energy loss function splits into two several portions such as high energy region and low energy region for the optical properties. It is related to energy loss,

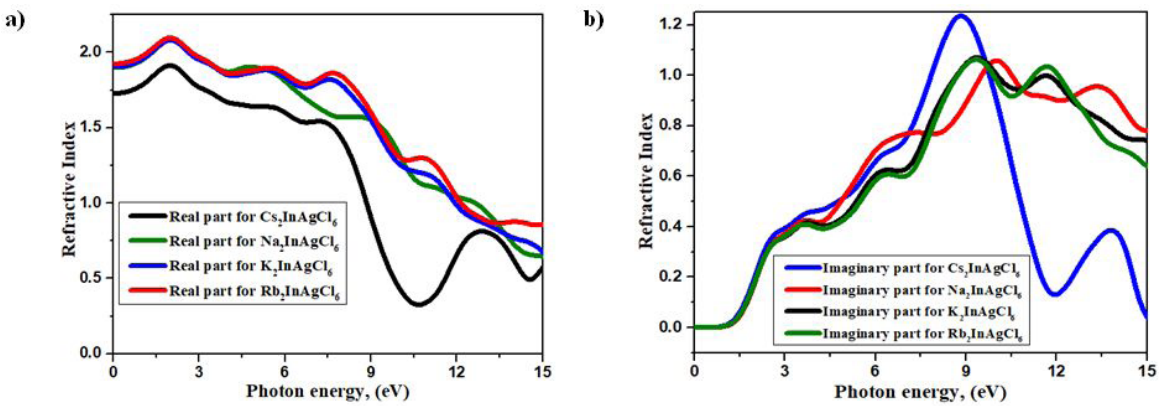

Figure 6. a) Refractive index (Real part), and b) Refractive index (Imaginary part).

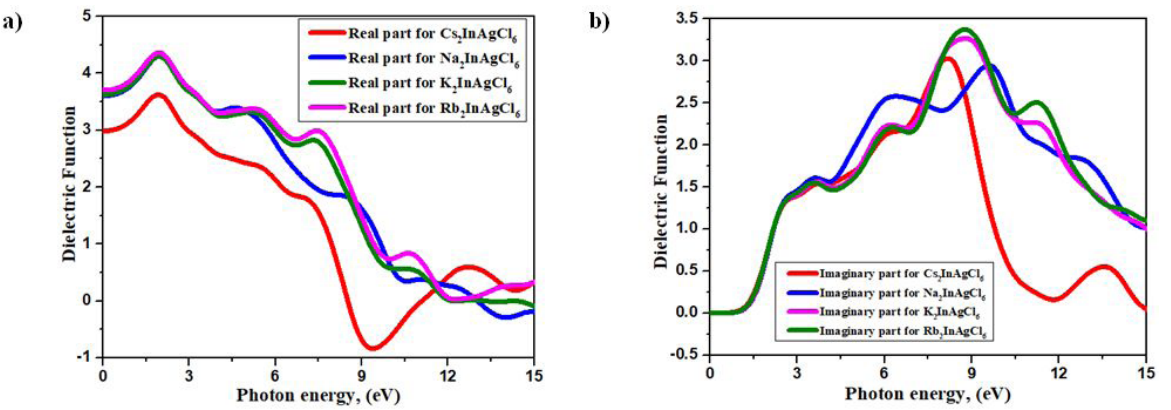

Figure 7. a) Dielectric function (Real part), and b) Dielectric function (Imaginary part).

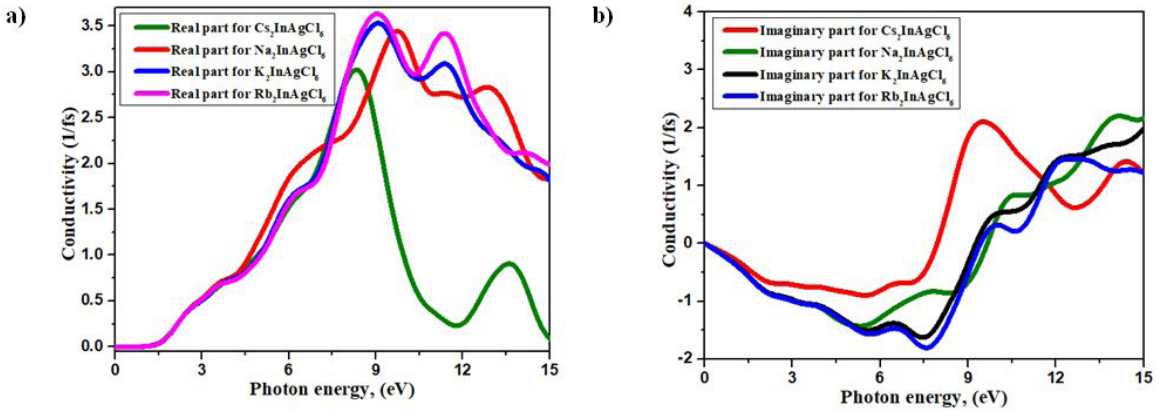

Figure 8. a) Conductivity (Real part), and b) Conductivity (Imaginary part).

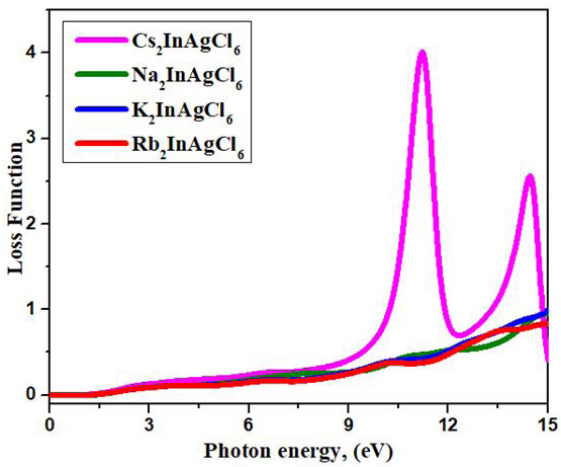

Figure 9. Loss Function.

momentum transfer and inelastic scattering characterization process. As can be seen in Figure 9 the first region after the ionizing edge is the high loss energy region with frequency or spectra change which can be called the oxidation state of d orbital fission for atomic metals of the nucleus in complex compounds, amounting to more than 18 eV. Before photon energy 15 eV, the comparative studies show that greater loss function for $Cs_2InAgCl_6$ than $Na_2InAgCl_6$, $K_2InAgCl_6$, and $Rb_2InAgCl_6$ respectively. After energy 10 eV, we found that for higher photon energy the loss function for $Cs_2InAgCl_6$ follows the highest loss function than $Na_2InAgCl_6$, $K_2InAgCl_6$, and $Rb_2InAgCl_6$. It may be revealed that $Cs_2InAgCl_6$ has illustrated the higher loss function in lower energy although it is almost zero after 10 eV and 14 eV.

4. Conclusion

It has been said that the methods of GGA with PBE, GGA with RPBE and LDA with CA-PZ have executed to evaluate the electronic band structure where the GGA with RPBE has considered as the most acceptance method to calculate band gap due to nearest value of experimental value. The calculated band gap of $Cs_2InAgCl_6$ is 1.310 eV through the GGA with RPBE while the experimental value is 1.370 eV. On the base structure of $Cs_2InAgCl_6$, $Na_2InAgCl_6$, $K_2InAgCl_6$, and $Rb_2InAgCl_6$ have been redesigned to make better perovskites cell materials which are lead free and smaller metals containing light materials, and shows low band gap than $Cs_2InAgCl_6$. These structures of free halide double perovskites contain the space group ($Fm\bar{3}m$) which is the most optimized and stable configuration, and it has reported the direct band gap in double perovskites. Our analysis indicates that by developing mixed halides $A_2InAgCl_6$ with A = Cs, Na, K, and Rb, it should be possible to obtain good optical absorbers, and good conductivity has demonstrated with direct band gap. From the part of loss function, one of the most significance has been found that the loss function of $Cs_2InAgCl_6$ is the highest among all while other three crystals show almost similar loss function. The conduction band of DOS has affected by Na, K and Rb atoms although the valance band is not a noticeable changed by these atoms so that it must be concluded about their electronic structure which depends on these atoms. The optical properties and electronic structure give the strong evidences for use of new functional materials in photovoltaic, photocatalysis, photo detectors, light-emitting devices, piezoelectric, and magneto electrics.

5. References

1. Zhao YZ, Zhu K. Organic-inorganic hybrid lead halide perovskites for optoelectronic and electronic applications. Chem Soc Rev. 2016;45(3):655-89.
2. Zhou JH, Huang J. Photodetectors based on organic–inorganic hybrid lead halide perovskites. Adv Sci. 2018;5(1):1700256.
3. Khan UZ, Zhinong Y, Khan AA, Zulfiqar A, khan QU. Organic-inorganic hybrid perovskites based on methylamine lead halide solar cell. Sol Energy. 2019;189:421-5.
4. Snaith HJ. Perovskites: the emergence of a new era for low-cost, high-efficiency solar cells. J Phys Chem Lett. 2013;4(21):3623-30.
5. Meng LY, You J, Yang Y. Addressing the stability issue of perovskite solar cells for commercial applications. Nat Commun. 2018;9(1):1-4.
6. Jacoby M. The future of low-cost solar cells. Chem Eng News. 2016;94(18):30-5.
7. Fu RZ, Zhou W, Li Q, Zhao Y, Yu D, Zhao Q. Stability challenges for perovskite solar cells. ChemNanoMat. 2019;5(3):253-65.
8. Wang RM, Mujahid M, Duan Y, Wang Z-K, Xue J, Yang Y. A review of perovskites solar cell stability. Adv Funct Mater. 2019;29(47):1808843.

9. Yang ZS, Song J, Zeng H, Wang M. Organic composition tailored perovskite solar cells and light-emitting diodes: perspectives and advances. Materials Today Energy. 2019;14:100338.
10. Zhang QS, Su R, Du W, Liu X, Zhao L, Ha ST, et al. advances in small perovskite-based lasers. Small Methods. 2017;1(9):1700163.
11. Li CL, Lu J, Zhao Y, Sun L, Wang G, Ma Y, et al. Highly sensitive, fast response perovskite photodetectors demonstrated in weak light detection circuit and visible light communication system. Small. 2019;15(44):1903599.
12. Lin QA, Armin A, Lyons DM, Burn PL, Meredith P. Low noise, IR blind organohalide perovskite photodiodes for visible light detection and imaging. Adv Mater. 2015;27(12):2060-4.
13. Gao PG, Grätzel M, Nazeeruddin MK. Organohalide lead perovskites for photovoltaic applications. Energy Environ Sci. 2014;7(8):2448-63.
14. Hailegnaw BK, Kirmayer S, Edri E, Hodes G, Cahen D. Rain on methylammonium lead iodide based perovskites: possible environmental effects of perovskite solar cells. J Phys Chem Lett. 2015;6(9):1543-7.
15. Yusoff ARMN, Nazeeruddin MK. Organohalide lead perovskites for photovoltaic applications. J Phys Chem Lett. 2016;7(5):851-66.
16. Boix PPA, Agarwala S, Koh TM, Mathews N, Mhaisalkar SG. Perovskite solar cells: beyond methylammonium lead iodide. J Phys Chem Lett. 2015;6(5):898-907.
17. Liu ZK, Krückemeier L, Krogmeier B, Klingebiel B, Márquez JA, Levcenko S, et al. Open-circuit voltages exceeding 1.26 V in planar methylammonium lead iodide perovskite solar cells. ACS Energy Lett. 2018;4(1):110-7.
18. Filip MRH, Hillman S, Haghighirad AA, Snaith HJ, Giustino F. Band gaps of the lead-free halide double perovskites $Cs_2BiAgCl_6$ and $Cs_2BiAgBr_6$ from theory and experiment. J Phys Chem Lett. 2016;7(13):2579-85.
19. Weng ZQ, Qin J, Umar AA, Wang J, Zhang X, Wang H, et al. Lead free $Cs_2BiAgBr_6$ double perovskite based humidity sensor with superfast recovery time. Adv Funct Mater. 2019;29(24):1902234.
20. Tran TT, Panella JR, Chamorro JR, Morey JR, McQueen TM. Designing indirect-direct bandgap transitions in double perovskites. Mater Horiz. 2017;4(4):688-93.
21. Volonakis GH, Haghighirad AA, Milot RL, Sio WH, Filip MR, Wenger B, et al. $Cs_2InAgCl_6$: a new lead-free halide double perovskite with direct band gap. J Phys Chem Lett. 2017;8(4):772-8.
22. Matsuyama T, Mukai M, Horinaka H, Wada K, Nakanishi T, Okumi S, Togawa K, Baba T. Photo-luminescence study of superlattice photocathode. In Proceedings of the 14th International Spin Physics Symposium. New York: American Institute of Physics; 2001.
23. Zhao JG, Guo C, Li T, Su X, Zhang N, Chen J. Synthesis, electronic structure and photoluminescence properties of $Ba_2BiV_3O_{11}$: Eu^{3+} red phosphor. Dyes Pigments. 2016;132:159-66.
24. Haque EH, Hossain MA. Electronic, phonon transport and thermoelectric properties of $Cs_2InAgCl_6$ from first-principles study. Computational Condensed Matter. 2019;19:e00374.
25. Ziesche PK, Kurth S, Perdew JP. Density functionals from LDA to GGA. Comput Mater Sci. 1998;11(2):122-7.
26. Kurth SP, John P. Molecular and solid state tests of density functional approximations: LSD, GGAs, and meta GGAs. Int J Quantum Chem. 1999;75(45):889-909.
27. del Campo JM, Gázquez JL, Trickey SB, Vela A. Non-empirical improvement of PBE and its hybrid PBE0 for general description of molecular properties. J Chem Phys. 2012;136(10):104108.
28. Yang K, Zheng J, Zhao Y, Truhlar DG. Tests of the RPBE, revPBE, tau-HCTHhyb, omegaB97X-D, and MOHLYP density functional approximations and 29 others against representative databases for diverse bond energies and barrier heights in catalysis. J Chem Phys. 2010;132(16):164117.
29. Perdew JPB, Burke K, Ernzerhof M. Generalized gradient approximation made simple. Phys Rev Lett. 1996;77(18):3865-8.
30. Howlader DH, Hossain MS, Chakma U, Kumer A, Islam MJ, Islam MT, et al. Structural geometry, electronic structure, thermo-electronic and optical properties of $GaCuO_2$ and $GaCu_{0.94}Fe_{0.06}O_2$: a first principle approach of three DFT functionals. Mol Simul. 2021;44:1-12.
31. Kumer A, Chakma U. Developing the amazing photocatalyst of $ZnAg_2GeSe_4$, $ZnAg_2Ge_{0.93}Fe_{0.07}Se_4$ and $ZnAg_2Ge_{0.8}6Fe_{0.14}Se_4$ through the computational explorations by four DFT functionals. Heliyon. 2021;7(7):e07467.
32. Al Mamun A, Monsur Alam M, Habib A, Chakma U, Sikder M, Kumer A. Structural, electronic, optical properties and molecular dynamics study of WO_3 $W_{0.97}Ag_{0.03}O_3$ and $W_{0.94}Ag_{0.06}O_3$ photocatalyst by the first principle of DFT study. Egypt J Chem. 2021;64(9):5117-26.
33. Ali M, Islam MJ, Rafid M, Jeetu RR, Roy R, Chakma U, et al. The computational screening of structural, electronic, and optical properties for SiC, Si0.94Sn0.06C, and Si0.88Sn0.12C lead-free photovoltaic inverters using DFT functional of first principle approach. Eurasian Chemical Communications. 2021;3(5):327-38.
34. Islam T, Kumer A, Chakma U, Howlader D. A computational investigation of electronic structure and optical properties of $AlCuO_2$ and $AlCu_{0.96}Fe_{0.04}O_2$: a first principle approach. Orbital Electron J Chem. 2021;13(1):58-64.
35. Jain AO, Ong SP, Hautier G, Chen W, Richards WD, Dacek S, et al. Commentary: The Materials Project: A materials genome approach to accelerating materials innovation. APL Mater. 2013;1(1):011002.
36. Parr RG, Szentpály L, Liu S. Electrophilicity index. J Am Chem Soc. 1999;121(9):1922-4.
37. Parr RGC, Pratim K. Principle of maximum hardness. J Am Chem Soc. 1991;113(5):1854-5.
38. Kumer A, Khan MW. Synthesis, characterization, antimicrobial activity and computational exploirations of ortho toludinium carboxylate ionic liquids. J Mol Struct. 2021;1245:131087.
39. Hoque MMH, Hussen MS, Kumer A, Khan MW. Synthesis of 5, 6-diaroylisoindoline-1, 3-dione and computational approaches for investigation on structural and mechanistic insights by DFT. Mol Simul. 2020;46(16):1298-307.
40. Kumer A, Khan MW. The effect of alkyl chain and electronegative atoms in anion on biological activity of anilinium carboxylate bioactive ionic liquids and computational approaches by DFT functional and molecular docking. Heliyon. 2021;7(7):e07509.
41. Nath A, Kumer A, Khan W. Synthesis, computational and molecular docking study of some 2, 3-dihydrobenzofuran and its derivatives. J Mol Struct. 2020;1224:129225. http://dx.doi.org/10.1016/j.molstruc.2020.129225.
42. Nath A, Kumer A, Zaben F, Khan MW. Investigating the binding affinity, molecular dynamics, and ADMET properties of 2, 3-dihydrobenzofuran derivatives as an inhibitor of fungi, bacteria, and virus protein. Beni-Suef Univ J Basic Appl. Sci. 2021;10(1):36.
43. Chakma U, Kumer A, Chakma KB, Islam MT, Howlader D, Mohamed RMK. Electronics structure and optical properties of $SrPbO_3$ and $SrPb_{0.94}Fe_{0.06}O_3$: a first principle approach. Eurasian Chem Commun. 2020;2(5):573-80.
44. Chakma U, Kumer A, Chakma KB, Islam MT, Howlader D. Electronics structure and optical properties of Ag_2BiO_3,$(Ag_2)_{0.88}Fe_{0.12}BiO_3$: a first principle approach. Adv J Chem A. 2020;3(4):542-50.
45. Hasan MM, Ajoy K, Unesco C. Theoretical investigation of doping effect of Fe for SnWO4 in electronic structure and optical properties: DFT based first principle study. Adv J Chem A. 2020;3(5):639-44.
46. Islam MT, Kumer A, Howlader D, Chakma KB, Chakma U. Electronics structure and optical properties of $Mg(BiO_2)_4$ and

$Mg(Bi_{0.91}Ge_{0.083}O_2)_4$: a first principle approach. Turkish Comput Theor Chem. 2020;4(1):24-31.

47. Kamal BC, Ajoy K, Unesco C, Debashis H, Tawhidul I. A theoretical investigation for electronics structure of $Mg(BiO_2)_2$ semiconductor using first principle approach. Int J New Chem. 2020;7(3):247-55.
48. Islam MJ, Kumer A. First-principles study of structural, electronic and optical properties of $AgSbO_3$ and $AgSb_{0.78}Se_{0.22}O_3$ photocatalyst. SN Appl Sci. 2020;2(2):251.
49. Bertsch GFI, Iwata J-I, Rubio A, Yabana K. Real-space, real-time method for the dielectric function. Phys Rev B Condens Matter Mater Phys. 2000;62(12):7998-8002.